The 2009 IEEE/RSJ International Conference on
Intelligent Robots and Systems
October 11-15, 2009 St. Louis, USA

Robots with Inflatable Links

Siddharth Sanan, Justin B. Moidel and Christopher G. Atkeson

***Abstract*—The use of robots in assistive roles will be an increasingly significant application for robotics. Assistive robots need to physically interact with humans in a safe manner. We propose the use of inflatable robot links as structural members instead of traditional rigid links. We believe such links would allow the development of inherently safe robots. For these robots to be useful in tasks such as assisting humans, it is essential that we be able to control contact forces with these robots. In this paper, we propose a model for force control with a single inflatable link, investigate the dynamics of the model, and present experimental results.**

I. Introduction

THIS paper presents a novel idea for making robots inherently safe using inflatable links. For safe physical human-robot interaction, there are essentially two requirements: a) safety under impact, b) safety under controlled interaction. Impact safety is characterized by the uncontrolled or open loop response of the system. We can relate this to the performance of the system under high frequency disturbances. Since typically any control system has a limited bandwidth of operation, no practical control system can modify this characteristic of the system. Safety under controlled interaction refers to the ability to control the interaction forces between the human and the robot within the bandwidth of the control system. This is what is typically referred to as force control. Fig. 1 shows the dependence of force on the frequency of interaction. At frequencies within the control bandwidth, interaction force is governed by the controller characteristics; while at higher frequencies, the interaction force is governed by the open loop characteristics of the system. During controlled interaction, the high frequency force disturbance is not large enough for concern. However during impact, this is not true; hence the open loop characteristics of the system become important from a safety perspective.

Techniques to evaluate safety in human-robot interaction have been proposed [1],[2]. Correspondingly, methods have been proposed for the design of safe rigid link robots [3]-[6]. However, even with careful design and sophisticated control, safety of rigid link robots is limited by the link mass and rigid structure. The rigid structure due to a hard surface (usually metal) results in high contact stiffness between the robot and the user. This is undesirable for safety [7]. Impact and continuous contact safety are directly addressed by the use of inflatable links which are extremely light and have much lower achievable contact stiffness. Padding the entire robot with soft material is also a solution but it has disadvantages such as causing the system to become bulky, heavy and causing mobility restrictions around joints.

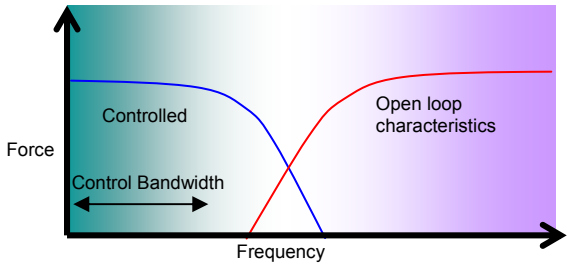

Fig. 1 Force interaction at various frequencies

The system being proposed is naturally safe under impact due to its low weight and contact stiffness. For the same reasons, air bags are used in vehicles. However, we need to establish the ability to do useful tasks using robots with inflatable links. One such ability is force control. We are in essence using inflatable links for their advantages under impact and attempting to extend their capability using force control. Inflatable structures were used in a robotic manipulator in [8]. To the best of the author's knowledge, the use of inflatable structures for force control is not previously documented. Force control with flexible link manipulators has been studied [9],[10]. We believe that the class of systems being investigated by us would operate under deflections which do not permit the use of a linear deflection model. We use a Pseudo Rigid Body Model (PRBM) [11] to analyze the system under large deflections.

This paper is organized as follows. In Section II, we describe the system we have developed and its model. Section III describes the behavior of the system as predicted by the model. In Section IV, we describe control schemes for force control, study the stability of the control based on Lyapunov Methods, and show experimental results. In Section V, we discuss issues and solutions to be implemented in the future, and finally in Section VI we present our conclusions.

II. Single Link Inflatable Robot

To study the use of inflatable links in robots, we prototyped a system consisting of a single inflatable link actuated at the base with a DC torque motor. Fig. 2 shows a photograph of the system and the schematic of the system is

Manuscript received July 31, 2009. This material is based upon work supported in part by the National Science Foundation under grants ECS-0325383, EEC-0540865, and ECS-0824077.

S. Sanan, J. B. Moidel and C. G. Atkeson are with the Robotics Institute, Carnegie Mellon University, Pittsburgh, PA 15213 USA (e-mail: sanan@cmu.edu, jmoidel@andrew.cmu.edu, cga@cmu.edu).

shown in Fig. 3. For this system, our goal is to be able to control the contact force exerted on the object by the inflatable link. We use the term inflatable beam and link interchangeably as the inflatable link in the system functions structurally as a beam.

Fig. 2. Single link inflatable robot

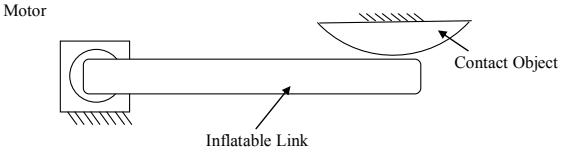

Fig. 3. Schematic of the system

The inflatable links we use in our system have been fabricated in our lab with polyurethane[1] sheets of varying thickness. The sheets are heat sealed to form an air tight chamber. We have also experimented with polyethylene sheets which did not give satisfactory results due to less structural load capacity, weak seals obtained, and formation of plastic regions after inflation. The lesser load capacity and formation of plastic regions can be related to the lower yield stress of polyethylene compared to polyurethane. The lower yield stress causes achievable pressures in the link to be smaller. Formation of plastic regions causes crimping of the link ultimately leading to lower structural capacity. For a polyurethane inflatable beam of length 50 cm, we were able to successfully carry a force of 8N at its end. The limitation in load capacity is largely due to certain prototyping issues. With this load capacity, the system can be used for applications such as manipulation of lightweight objects and grooming which have small force requirements and are relevant to people needing assistance in activities of daily living (ADLs). Higher load capacities on the order of a few hundred Newtons can be achieved as is shown in [13],[14].

Inflatable beams are different from traditional beams as the material used to make them can only hold tensile stress. An inflatable tube can be modeled in a number of ways suggested in [11]-[13]. The simplest approach is to consider the effect of pressure in the tube as a pre-stress in the tube. Then the Euler-Bernoulli beam theory for large deflections can be applied to obtain deflections and stresses in the beam. The beam fails when the stress at any point on the surface of the beam is less than zero. In the following subsections, we discuss a system model and system behavior.

[1] Source: McMaster-Carr, Catalogue # 3460

A. Large Deflection Beam Analysis

In the following discussion, we review some theory about large deflections of solid beams to understand the deflection characteristics of an inflatable beam. We assume the beam is inextensible and consider only geometric nonlinearity. For the sake of simplicity, we study a cantilever beam with a moment load (M_0) at its end for large deflections.

We know from Euler-Bernoulli beam theory:

$$\frac{d\theta}{ds} = \frac{M_0}{EI} \tag{1}$$

$$\frac{d\theta}{ds} = \frac{d^2y/dx^2}{(1+(dy/dx)^2)^{3/2}} \tag{2}$$

where, E is the Young's Modulus of the beam material, I is the area moment of the cross section of the beam, s is the arc length along the beam, θ is the angle of the tangent to the beam from the horizontal, y is the transverse deflection of the beam which is a function of the position x along axial direction. In linear analysis, we say the slopes in (2) are small and neglect its powers and get the standard equation. For the large deflection case, the powers of the slope cannot be neglected. Therefore we start with (1) and integrate along the arc length s, for the length L of the beam.

$$\int_0^{\theta_0} d\theta = \int_0^L \frac{M_0}{EI} ds \tag{3}$$

$$\Rightarrow \theta_0 = \frac{M_0 L}{EI}$$

Hence the angular deflection at the end of the beam, with no small deflection assumptions, is given by (3). From (3), the relationship between angular deflection and moment at the end of the beam is linear. Such a relation allows for a simple representation of a flexible link with sufficient accuracy using only a few parameters as discussed in the next subsection. Such simplifications are also possible for beams with other loading conditions. For a detailed analysis of beams with end loads and large deflection, see [15].

B. Pseudo Rigid Body Model

The rigid body model allows the representation of large deflections of flexible systems by rigid bodies and spring elements. For instance, the large deflections of the beam described in the previous subsection can be modeled as shown in Fig. 4. The model is defined by the following parameters: r defines the distance of the hinge from the fixed end of the beam, l is the length of the beam, K is the spring constant of the torsional spring at the hinge, θ is the angular deflection of the torsional spring, f is the force at the end of the beam and y is the vertical deflection at the end of the beam.

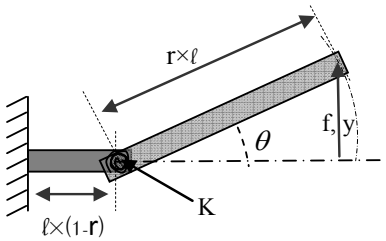

Fig. 4. Parameters of the pseudo rigid body model of the link

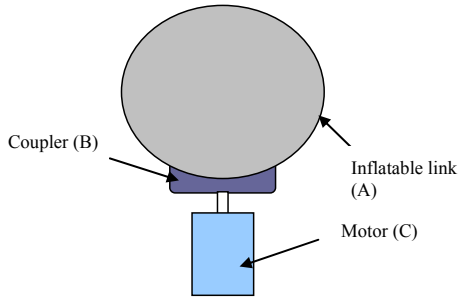

Fig. 5. Schematic showing the components of the system looking into the cross section of the inflatable link

The rigid body model consists of two bodies connected by a hinge through a linear torsional spring. Since inflatable links used in serial robots are essentially beams with pre-stress due to internal pressure, we shall model the inflatable link using the rigid body model. Fig. 5 shows the components of the system being studied. For the experimental deflection testing discussed in the next section, a coupler B is fixed. The coupler B is attached to the link by the use of polymer adhesives and thermal welding.

C. *Experimental Deflection Testing*

To fit a rigid body model described in previous subsections to the inflatable beams fabricated by us, we conducted deflection tests. Fig. 4 shows the rigid body model that is fit to the system for deflection modeling. The inflatable beam was fixed at one end and weights were hung at the other end of the beam.

For the system, we have the following relation between load f and deflection y:

$$f_i(rl)\cos\theta_i = K\theta_i + c$$
$$\Rightarrow [K,c]^T = \left(A^T A\right)^{-1} A^T (Frl) \tag{4}$$

where

$$\theta_i = \sin^{-1}\left(\frac{y_i}{l_i}\right)$$
$$A_{i,1} = \theta_i, A_{i,2} = 1$$
$$F = \left[f_1 \cos\theta_1, f_2 \cos\theta_2 ..., f_n \cos\theta_n\right]^T$$

K is the best linear least squares stiffness for the load deflection data and the offset c is the moment value at zero deflection. The value of r is taken from the literature [15] to be equal to 0.8517. In the experiments, we measure the tip displacements and we need to find the equivalent torsional stiffness K of the beam. Table 1 gives a sample of the load-deflection data. The value of K and c obtained from the data is 3.8576 N·m/rad and 0.1205 respectively. It is to be noted c is not forced to zero (which would be the case in the absence of unmodeled physical phenomena, errors in the position/force readings, etc.) to get a more accurate approximation of K.

TABLE I
LOAD DEFLECTION DATA FOR INFLATABLE BEAMS

y (mm)	Load (N)
0.6	6
1.1	12
2.6	32
3.7	54
4.3	62
5.0	72
5.6	84

The linear least squares fit of the form given in (4) is shown along with experimental data in Fig. 6. Although we obtained a linear torsion spring constant K for the deflection model of the inflatable beam, for generality, we shall use a spring with moment-angular deflection relation given by (5) in further analysis.

$$\tau = k_1\theta + k_2\theta^3 \tag{5}$$

Equation (5) is useful if in addition to geometric nonlinearities, other nonlinearities due to material properties, motor-link coupling and other unmodelled effects in the system exist. In fact for all the analysis presented in subsequent sections, (5) can be replaced by any higher order function of the angular deflection as well, without affecting the validity of the analysis.

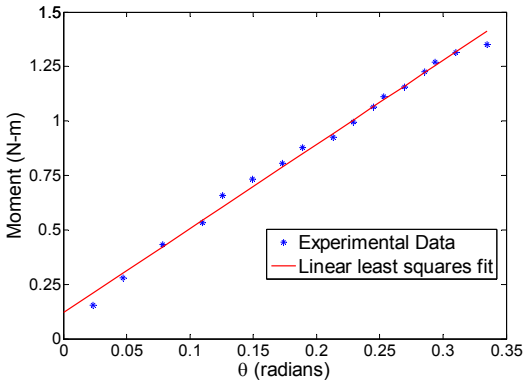

Fig. 6. Linear spring fit to the load deflection data

III. SYSTEM MODEL AND BEHAVIOR

To develop our control, we propose a rigid body model of the system as shown in Fig. 7. Since we have an inflatable link which has high surface compliance, a linear contact spring k_s is a suitable choice. From the model, it can be seen that the system resembles a series elastic actuator (SEA) [3].

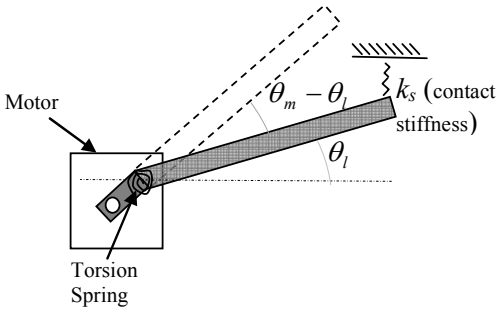

Fig. 7. Rigid body model of the system

The rigid link in our model can be considered massless as we have an inflatable link and its mass can be neglected. The only source of inertia is the motor inertia (J_m).

The equations for the system are given by:

$$J_m\ddot{\theta}_m + k_1(\theta_m - \theta_l) + k_2(\theta_m - \theta_l)^3 + b(\dot{\theta}_m - \dot{\theta}_l) = T_m \tag{6}$$

In (6), T_m is the input torque to the motor, k_1 and k_2 are torsional stiffness coefficients of the spring, b is the viscous damping coefficient, θ_m and θ_l are described in Fig. 7. Further the torque due to contact with the object, T_L is given by (7):

$$\begin{aligned} T_L &= \frac{k_s l_c^{\,2}\sin 2\theta_l}{2} + k_s l_c(l - l_c)\sin\theta_m \cos\theta_l \\ &\approx \frac{k_s l_c^{\,2}\sin 2\theta_l}{2} = k_1(\theta_m - \theta_l) + k_2(\theta_m - \theta_l)^3 + b(\dot{\theta}_m - \dot{\theta}_l) \end{aligned} \tag{7}$$

assuming $\frac{k_s l_c^{\,2}\sin 2\theta_l}{2} >> k_s l_c(l - l_c)\sin\theta_m \cos\theta_l$.

Here $l_c = rl$ and r is very close to 1. Note that from (7), T_L is a function of θ_l. Further we define the torque T_N at any deflection as:

$$T_N(\theta_m - \theta_l) = k_1(\theta_m - \theta_l) + k_2(\theta_m - \theta_l)^3 \tag{8}$$

Using (6) and (7), we can obtain the state space form of the dynamics equations:

$$\begin{aligned} \dot{x}_1 &= x_2 \\ \dot{x}_2 &= \frac{1}{J_m}\left(T_m - \frac{k_s l_c^{\,2}\sin 2x_3}{2}\right) \\ \dot{x}_3 &= \frac{1}{b}\left(k_1(x_1 - x_3) + k_2(x_1 - x_3)^3 + bx_2 - \frac{k_s l_c^{\,2}\sin 2x_3}{2}\right) \end{aligned} \tag{9}$$

where, $x_1 = \theta_m, x_2 = \dot{\theta}_m, x_3 = \theta_l$.

A. System Behavior

The system described by (9) was simulated with an input $u = T_m = 1$. Fig. 8 describes the response with time. For the step input $T_m = 1$ applied at $t = 0$, the system exhibits stable characteristics as can be seen from the response.

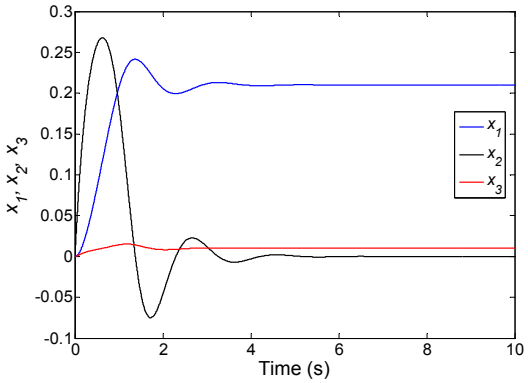

Fig. 8. Step response of the system

B. Lyapunov Stability Analysis

We use the Lyapunov method for studying the stability of the system [16]. For understanding the stability properties of the system, we take the candidate Lyapunov function V as:

$$V = \frac{1}{2}x_2^{\,2} + \int_0^{x_1 - x_3} T_N(\sigma)d\sigma + \int_0^{x_3} T_L(\sigma)d\sigma \tag{10}$$

V is a positive definite function as each of the terms involving the spring stiffness integrates to positive values. Here T_L and T_N were defined in (7) and (8) respectively.

Differentiating (10), we get:

$$\dot{V} = x_2\dot{x}_2 + T_N(x_1 - x_3)(\dot{x}_1 - \dot{x}_3) + T_L(x_3)\dot{x}_3 \tag{11}$$

Using (7) and (8) in (11),

$$\begin{aligned} \dot{V} &= -bx_2^{\,2} + 2bx_2\dot{x}_3 - b\dot{x}_3^2 + x_2 u \\ &= -b(x_2 - \dot{x}_3)^2 + x_2 u \end{aligned} \tag{12}$$

As can be seen from (12), for the open loop response i.e. when $u = 0$, $\dot{V} \le 0$. Therefore as can be seen from Fig. 8, the system is stable. Further, asymptotic stability can be proved by invoking LaSalle's theorem. For the closed loop system, the control law u needs to be chosen to ensure stability in the Lyapunov sense.

IV. Force Control

Considering the system behavior, there are a number of options regarding what states we need to measure and the states we want to control. We shall explore two sensing options: a) place an encoder at the motor which gives the motor angle, b) place a force sensor at the contact tip to measure the contact force. We desire to maintain a constant reference force F_d given by:

$$\begin{aligned} F_d &= y_d = k_s l_c \sin(x_{3d}) \\ \Rightarrow x_{3d} &= \sin^{-1}(F_d / k_s l_c) \end{aligned} \tag{13}$$

The set point input u_s is:

$$u_s = \frac{k_s {l_c}^2 \sin 2\theta_{3d}}{2} \tag{14}$$

This shifts the equilibrium to the desired state and all equations are now with respect to this equilibrium.

A. Motor Encoder

Here we measure the motor shaft angle x_1 and velocity x_2. It should be noted that we can use the motor encoder to control the contact force for a static object only. For moving contact objects, we would need another sensor to inform us about the position of the contact object. The output of the system is given by:

$$\bar{y} = \begin{bmatrix} x_1 & x_2 \end{bmatrix}^T \tag{15}$$

We choose the PD control law:

$$u = k_p(-x_1) + k_v(-x_2) \tag{16}$$

We modify the Lyapunov function V to V' such that

$$V' = \frac{1}{2}{x_2}^2 + \int_0^{x_1 - x_3} T_N(\sigma)d\sigma + \int_0^{x_3} T_L(\sigma)d\sigma + \frac{1}{2}k_p {x_1}^2 \tag{17}$$

Again differentiating (17) with time,

$$\begin{aligned} \dot{V}' &= -b(x_2 - \dot{x}_3)^2 + x_2 k_p(-x_1) + x_2 k_v(-x_2) + k_p x_1 x_2 \\ &= -b(x_2 - \dot{x}_3)^2 - k_v {x_2}^2 \end{aligned} \tag{18}$$

Clearly, $\dot{V}' \le 0$. Hence the system is stable in the sense of Lyapunov. Fig. 9 and Fig. 10 show the simulation of the above system.

B. Contact Force Sensor

Here we place a force sensor at the contact point and measure the contact force. We assume that the contact force lies in the plane of the actuation torque from the motor.

The output of the system is given by:

$$y = k_s l_c \sin(x_3) \tag{19}$$

The proposed control law u is:

$$u = k_p(-y) \tag{20}$$

Using (20) in (12),

$$\begin{aligned} \dot{V} &= -b(x_2 - \dot{x}_3)^2 + x_2 k_p(-y) \\ &= -b(x_2 - \dot{x}_3)^2 - x_2 k_p k_s l_c \sin(x_3) \end{aligned} \tag{21}$$

From (21), stability of the system is unclear. It can be observed that if $x_3 << x_2$, then $\dot{V} < 0$. However if k_p is increased to a sufficiently large value, $\dot{V}$ may not remain negative semi-definite and the system may become unstable. Fig. 11 shows the advantage of using force feedback in terms of convergence to the desired force level.

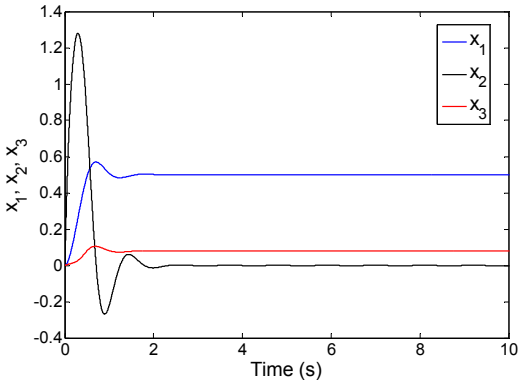

Fig. 9. Model states in simulation with PD control on motor angle

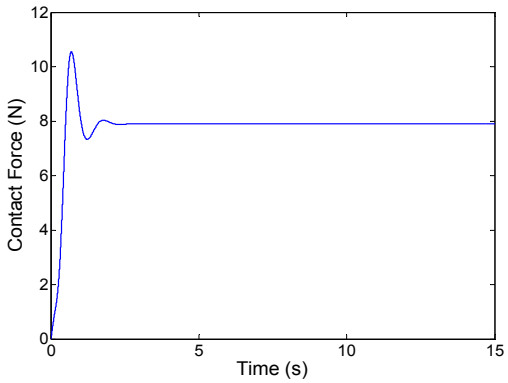

Fig. 10. Contact force in simulation with PD control on motor angle

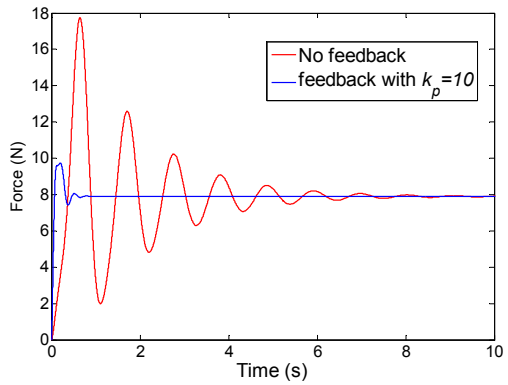

Fig. 11. Contact force in simulation with and without feedback

C. Experimental Results

Experiments using the system shown in Fig. 2 were performed. The system comprises of an inflatable link actuated at the base using a DC torque motor, a 500 CPR Motor Encoder and a Honeywell Force Sensor[2]. It should be noted that the range of forces applied to the link was limited in the experiments due to actuation limitations. Hence for the experiments, we operated only under small deflections of the beam. Control sampling frequency was 100 Hz. Fig. 12 and Fig. 13 show the contact force evolution for different desired force values using PID control on motor position and force sensor feedback respectively.

[2] Honeywell FSG15N1A

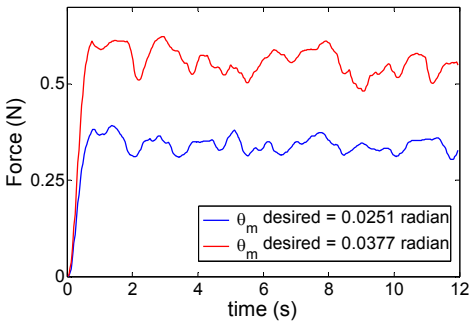

Fig. 12. Force at the contact point due to position control on motor

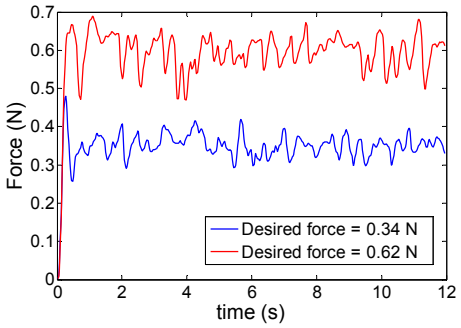

Fig. 13. Force at the contact point due to force feedback

V. Discussion

The use of a single contact force sensor allows the contact force to be controlled over the assumed contact point only. Using printed strain gages on the polymer used to fabricate the inflatable link allows the possibility of aggregate force sensing and multi-contact point force sensing. This would enable force control while contacting an external object with the inflatable link at any point on it.

For our system, we consider force in a single plane only. Extension of force sensing and control to all 3 dimensions needs to be addressed. The system we described has a single active degree of freedom, therefore we can actively control force in a single direction only. We can increase the degrees of freedom in two ways: a) using multiple inflatable links, b) achieving motion through elastic deflection of the link in 3D. We have recently prototyped a system utilizing the latter method, the description of which would be presented in a future publication. Creases caused due to sealing and flexural hinges made by introducing a narrow section between links could replace traditional hinges when multiple inflatable links are to be used. The design could involve the use of a robot structure that is either entirely inflatable or inflatable near the end effector of the robot. Inflatable structures could also be used as end effectors in the form of grippers. Beyond safety, these systems could also offer advantages of a deployable structure, accessibility in convoluted environments and a non-metallic structure suitable for applications such as image-guided surgery.

VI. Conclusion

A novel solution to making robots safe by the use of inflatable robot links has been proposed. Safety of such a system in environments involving humans is seen as the primary advantage of such a system. To extend the usefulness of such a system in robotic tasks such as manipulation and physical interaction with humans, force control for such a system was developed. Experiments with the system show stable contact force levels can be achieved with the system.

References

[1] S. Haddadin, A. Albu-Schaffer, and G. Hirzinger, "Safety evaluation of physical human-robot interaction via crash testing," *Robot. Sci. Syst. Conf.*, 2007.

[2] S. Haddadin, A. Albu-Schaffer, and G. Hirzinger, "Safe physical human-robot interaction: measurements, analysis & new insights," *Int. Symp. Robot. Res.*, 2007.

[3] D. W. Robinson, J. E. Pratt, D. J. Paluska, and G. A. Pratt, "Series elastic actuator development for a biomimetic walking robot," *Proc. IEEE/ASME Int. Conf. Advanced Intelligent Mechatronics*, pp. 561-568, 1999.

[4] M. Zinn, O. Khatib, and B. Roth, "A new actuation approach for human friendly robot design," *Proc. IEEE Int. Conf. Robotics & Automation*, vol. 1, pp. 249-254, 2004.

[5] G. Hirzinger, N. Sporer, A. Albu-Schaffer, M. Hahnle, R. Krenn, A. Pascucci, and M. Schedl, "DLR's torque-controlled light weight robot III - Are we reaching the technological limits now?," *Proc. IEEE Int. Conf. Robotics & Automation*, vol. 2, pp. 1710-1716, 2002.

[6] R. Schiavi, G. Grioli, S. Sen, and A. Bicchi, "VSA-II: A novel prototype of variable stiffness actuator for safe and performing robots interacting with humans," *Proc. IEEE Int. Conf. Robotics & Automation*, pp. 2171-2176, 2008.

[7] J. Hutchinson, M. J. Kaiser, and H. M. Lankarani, "The Head Injury Criterion (HIC) functional," *J. Appl. Math. Comput.*, vol. 96, no. 1, pp. 1-16, 1998.

[8] N. Salomonski, M. Shoham, and G. Grossman, "Light Robot Arm Based on Inflatable Structure," *CIRP Annals Manufacturing Technology*, vol. 44, no. 1, pp. 87-90, 1995.

[9] J. L. Chang, and Y. P. Chen, "Force control of a single-link flexible arm using sliding-mode theory," *J. Vib. Cont.*, vol. 4, no. 2, pp. 187-200, 1998.

[10] B. C. Chiou, and M. Shahinpoor, "Dynamic stability analysis of a one-link force-controlled flexible manipulator," *J. Rob. Sys.*, vol. 5, no. 5, pp. 443-451, 1998.

[11] L. L. Howell, A. Midha, and T. W. Norton, "Evaluation of equivalent spring stiffness for use in a pseudo-rigid-body model of large-deflection compliant mechanisms," *J. Mech. Des.*, vol. 118, no. 1, pp. 126-131, 1996.

[12] J. D. Suhey, N. H. Kim, and C. Niezrecki, "Numerical modeling and design of inflatable structures-application to open-ocean-aquaculture cages," *J. Aquacultural Engg.*, vol. 33, no. 4, pp. 285-303, 2005.

[13] S. L. Veldman, *Design and Analysis Methodologies for Inflated Beams*. Delft University Press, 2005.

[14] A. V. Le, and C. Wielgosz, "Bending and buckling of inflatable beams: Some new theoretical results," *J. Thin-Walled Struct.*, vol. 43, no. 8, pp. 1166-1187, 2005.

[15] L. L. Howell, *Compliant Mechanisms*. Wiley-IEEE, 2001.

[16] J. E. Slotine, and W. Li, *Applied Nonlinear Control*. New Jersey: Prentice Hall, 1991.